

Lawrence Berkeley National Laboratory

LBL Publications

Title

Theoretical Relations between Electronic and Ionic Work Functions, Standard Reduction Potentials for Metal Dissolution and the Corrosion Potential

Permalink

<https://escholarship.org/uc/item/24d5f892>

Journal

Journal of The Electrochemical Society, 169(8)

ISSN

0013-4651

Authors

Li, Sirui
Frankel, Gerald S
Taylor, Christopher D

Publication Date

2022-08-01

DOI

10.1149/1945-7111/ac86f8

Copyright Information

This work is made available under the terms of a Creative Commons Attribution License, available at <https://creativecommons.org/licenses/by/4.0/>

Peer reviewed

Theoretical Relations between Electronic and Ionic Work Functions, Standard Reduction Potentials for Metal Dissolution and the Corrosion Potential

To cite this article: Sirui Li *et al* 2022 *J. Electrochem. Soc.* **169** 081506

View the [article online](#) for updates and enhancements.



ECS Membership = Connection

ECS membership connects you to the electrochemical community:

- Facilitate your research and discovery through ECS meetings which convene scientists from around the world;
- Access professional support through your lifetime career;
- Open up mentorship opportunities across the stages of your career;
- Build relationships that nurture partnership, teamwork—and success!


Join ECS!

Visit electrochem.org/join





Theoretical Relations between Electronic and Ionic Work Functions, Standard Reduction Potentials for Metal Dissolution and the Corrosion Potential

Sirui Li,¹  Gerald S. Frankel,^{1,*} and Christopher D. Taylor^{1,2,z}

¹Fontana Corrosion Center, Department of Materials Science and Engineering, The Ohio State University, Columbus, Ohio 43210, United States of America

²Materials Technology & Development, DNV, Dublin, Ohio 43017, United States of America

Corrosion resistance has become an important factor to consider in integrated computational materials engineering, yet generating science-based indicators of corrosion resistance for hypothetical materials remains challenging. We explore the quantitative relations between work function and corrosion potential, taking a theoretical approach that considers the relation between these thermodynamic and kinetically-determined variables. The work function is a fundamental thermodynamic property of a metallic surface in isolation, whereas the corrosion potential is kinetically determined as the potential at which the rates of anodic and cathodic processes active on the metal surface are equal. The latter quantity is therefore time dependent, as well as dependent on the material, surface preparation, ageing/history and the environment. Reasoning from Mixed Potential Theory, we develop a rationale for the correlation between the corrosion potential and the electronic work function. Two distinct Born-Haber cycles for the anodic dissolution reaction are analyzed to allow calculation of a related quantity, the ionic work function, which embodies the energy of desorption for metal cations from an electrode. The ionic work function is not only highly correlated with, but of similar magnitude to the cation hydration energy. The theoretical analysis provided herein establishes the significance of not only the electronic work function, but also the ionic work function, cation hydration energy, cohesive energy and the ionization potential as co-descriptors for the corrosion resistance of candidate corrosion resistant metal alloys, with the role of the environment to be considered in future work.

© 2022 The Electrochemical Society ("ECS"). Published on behalf of ECS by IOP Publishing Limited. [DOI: [10.1149/1945-7111/ac86f8](https://doi.org/10.1149/1945-7111/ac86f8)]

Manuscript submitted March 2, 2022; revised manuscript received June 28, 2022. Published August 25, 2022.

Supplementary material for this article is available [online](#)

Developing a scientific framework that can reconcile the insights gained from the increasingly high-resolution window into atomic, molecular and microstructural processes afforded by modern experimental characterization and theoretical modeling techniques with respect to the macroscopic corrosion performance of a material in a given environment remains a considerable challenge for the corrosion science community. To address this challenge, two schools of thought have emerged. One contemporary approach leverages the collective power of data analytics, multiscale modeling, and multi-physics simulation to enhance the value of experimental datasets. In this approach, featurization is used to dis-aggregate corrosion into its constituent microprocesses, relating microprocess descriptors to characteristics of the materials and environment. In this way, a series of single-valued descriptors representing key metrics related to materials composition, microstructure, electronic and chemical properties, as well as the target environment(s) are collected in a repository.¹ These features may then be analyzed via machine learning to predict corrosion performance metrics, like corrosion potential, corrosion current density, passive current density, pitting potential, repassivation potential, etc.²

In contrast to this semi-empirical descriptor-based approach is the deterministic approach. A deterministic model uses first principles to reconstruct the electronic, atomistic, mesoscale, and continuum structure of the materials/environment interface with the aim of representing a real-world system with sufficient and necessary fidelity. As an example, one could try to simulate from a first principles approach, like density functional theory, the current density vs electrochemical potential curve associated with the corrosion of an alloy surface using only potential-dependent rate constants and thermodynamic factors inferred from electronic structure. This methodical approach would evolve through the gradual incorporation of more relevant physical and chemical features such as the variety of crystallographically oriented surface planes,³ defects,⁴ grain

boundaries, microstructural features,^{3,5,6} electrochemical double layer effects,^{7,8} etc. and therefore would be an extraordinarily challenging, complex and time-consuming although impressive endeavor.

In either approach, one must connect the result of physics-based simulations to a set of descriptors that can feed into the data analytics, or become useful parameters for thermodynamic and kinetic modeling. In recent times, various computable parameters that can be gleaned from first-principles calculations have been proposed for these endeavors such as activation energies for surface process like hydrogen recombination or water dissociation,⁹ adsorption energies for chloride or oxide anions and the related chloride susceptibility index,^{10,11} cohesive energies for surface atoms,^{12,13} surface energies for various low-index surfaces,⁴ formation energies of ions in solution,¹⁴ and the electronic work function.¹⁵ Re-examination of the classic and contemporary literature has prompted us to consider the electronic work function in particular. The electronic work function is a key indicator of the depth of the inherent stability of an electron within a given metal.^{16–18} It is then feasible that the electronic work function could be calculated for various alloys, intermetallic particles, surface planes, etc. and used to infer their relative electrochemical activity with respect to corrosion, since corrosion involves the simultaneous loss of electrons and ions from a metallic system. Whereas this makes intuitive sense, we also must keep in mind that corrosion is fundamentally a kinetically controlled process governed by various interconnected microkinetic mechanisms related to surface adsorption, molecular recombination, charge transfer and mass-transport across electrified interfaces. Therefore, a mathematical connection between the intrinsic work function of a material and its measurable corrosion performance is not obvious *a priori*, despite the intuitive appeal. In the work that follows, we consider in some depth a theoretical and empirical basis for using the work function as a descriptor, applying thermodynamic cycles to consider the nature of this connection and its relationship to another key descriptor that is re-discovered in this work along the way, namely, the ionic work function.

*Electrochemical Society Fellow.

^zE-mail: Christopher.taylor@dnv.com

Theoretical Model Development

The significance of the work function in corrosion and electrochemistry.—The electronic work function, ϕ_e , is a fundamental surface property that measures the energy required to bring an electron from the Fermi level to a point of rest just outside the surface.^{16–18} For metals, ϕ_e is interpreted as the electron's electrochemical potential,¹⁹ where the chemical contribution originates from the chemical potential gradient between a point inside and another point outside the metal in vacuum, and a contribution from the electrostatic interaction between electrons and metal ions. The two contributions are deemed to be inseparable.²⁰ In fundamental research, ϕ_e has been used as a convenient descriptor, as it has been found to be correlated with multiple physical quantities of interest. For example, Trasatti reported a linear correlation between the electronegativity (using the Pauling scale) and ϕ_e .²¹ This correlation can be improved by separating the class of metals into *sp* group metals and *d* group metals. With updated ϕ_e data, Michaelson reported a similar linear correlation using the Mulliken scale to describe electronegativity.²² From the linear correlation, Michaelson pointed out that solids, an ensemble of aggregating individual atoms, retain characteristics of their atomic origin.²²

Regarding electrocatalysis, Kita and Kurisu collected exchange current densities for hydrogen evolution on various metal substrates and found a linear correlation with the ϕ_e .²³ It is not surprising to find that metals with the highest ϕ_e (e.g. Pt, Pd) also possess the best catalytic activity to facilitate hydrogen evolution, since metals with higher ϕ_e are electrochemically more noble and form a stable substrate for facilitating molecular bond breaking and re-forming processes than metals with lower ϕ_e . Metals with lower ϕ_e , on the other hand, are generally more electrochemically reactive, in which case, electrochemical catalysis reaction occurs in parallel with metal dissolution, i.e. corrosion.

Concerning electrochemical and typically aqueous corrosion, it is generally accepted that ϕ_e is a useful parameter to assess materials' intrinsic nobility and electrochemical reactivity. The operating principle of the Kelvin probe relies, in part, on the concept of ϕ_e .²⁴ When two metals composed of different elements are brought into electrical contact, electrons flow from the metal with lower ϕ_e to the other metal with higher ϕ_e until the two metals' Fermi levels are aligned, and a state of electrochemical equilibrium is achieved. An electrostatic potential gradient will be built up in the space between the sample and the probe, and the total potential difference of this gradient is known as the Volta potential difference, which equals the difference of the ϕ_e between the sample and the probe. To measure the Volta potential difference, the Kelvin probe applies an external backing voltage to null the signal, and the Volta potential difference equals the backing potential when the signal goes to zero. Stratmann introduced the Kelvin probe technique to the study of corrosion and showed that there exists a linear correlation between Volta potential difference and the corrosion potential, E_{corr} .²⁴ Schmutz and Frankel demonstrated the utility in corrosion research of Scanning Kelvin Probe Force Microscopy (SKPFM),²⁵ which combines the functionality of SKP with the scanning abilities of atomic force microscopy (AFM).²⁶ In a typical operation of the SKPFM, a sample surface is first probed with a cantilever in the AFM mode to gather information on surface features. Following the AFM mode scan, the probe is then fixed in distance relative to the surface at approximately 100 nm, where SKP mode can perform Volta potential mapping. In corrosion research, SKPFM can be used to gain micrometer level information of a surface with heterogeneous features (e.g., intermetallic particles). Schmutz and Frankel demonstrated that SKPFM can be a suitable tool to characterize aluminum alloys AA2024-T3, where the presence of intermetallic particles is abundant and causes localized corrosion.²⁵ This study reported a linear correlation between Volta potential and E_{corr} measured immediately after the sample is emersed from solution.²⁵

Volta potential of a surface undergoing corrosion is related to the surface charge, which is mainly composed of dissolved metal cations, solute ions, and solvent dipoles and moderated by the substrate metal work function. The complex relationship between the measured Volta potential difference and E_{corr} was explored by Rohwerder and Turcu.²⁷ In their assessment, the Volta potential difference relates to the ϕ_e difference between the sample surface and reference tip, which should be an absolute quantity, whereas E_{corr} also depends on the interaction between metal and solution, thereby encompassing the solution chemistry, pH, solvent dipole orientations, etc. Furthermore, E_{corr} is both fundamentally and in a practical sense a kinetically controlled quantity, whereas ϕ_e is fundamentally thermodynamic. Yet a relationship exists between the two quantities, as has been observed and utilized in previous works.^{4,21,28–32}

In this communication, we explore the correlation and theoretical connections between the three related quantities of the corrosion potential (E_{corr}), the standard electrode potential ($E_{\text{red}}^0/E_{\text{ox}}^0$) and ϕ_e . Following Rohwerder and Turcu,²⁷ we focus on the processes of charge transfer occurring at the metal and solvent interface and at the metal and vacuum interface, from which Gerischer has argued that the standard free energy of the electron in the electrolyte must be equivalent to the Fermi level in the solid, E_{F} .³³ Accordingly, the Fermi level in the redox system may be correlated to the reduction potential of the redox couple through the expression:³³

$$E_{\text{F}} = -eE_{\text{red}}^0 + \text{Constant} \quad [1]$$

By collecting ϕ_e published by Michaelson and others,^{34,35} we explore the fidelity of Gerischer's conjecture. In the accompanying theoretical analysis, which uses a Born-Haber cycle to construct a linear relation between ϕ_e and E_{red}^0 , the concept of the ionic work function, $\phi_{\text{M}^{n+}}$, naturally emerges and is shown to be another potential descriptor with significance to metal dissolution.

Relating the work function to the corrosion potential via mixed potential theory.—The corrosion potential (E_{corr}) is the electrochemical potential at which the anodic current produced from a dissolving metal (i.e. the anodic oxidation reaction) becomes equal to the cathodic current produced from the counter reduction reaction that consumes those electrons.^{31,36,37} Whereas this is effectively a parameter that can only be determined by a comprehensive mapping of the kinetics of the electrochemical reactions that are operative on any given electrode surface (and may be heterogeneous across the surface and rapidly changing with time, which can also be true for the environment phase close to the interface), it is also undeniably influenced by thermodynamic driving forces characteristic to the material and environment. These thermodynamic driving forces include the difference in thermodynamic stabilities of the metallic and aqueous states of the metal (i.e. the standard reduction potential for the metal), the driving force for the cathodic evolution reactions (i.e. the standard reduction potential for the cathodic reactions), the thermodynamic contributing factors for the defect states present in the metal (i.e. surface energies for various surface planes, surface vacancy formation energies on terraces, steps and kinks, grain boundary interface energies, etc.), the ionic and electronic work functions that indicate the resistance to charge transfer for ions and electrons, respectively, and the cohesive energies (E_{coh}) of various matrix, secondary and precipitate phases that form in the microstructure. A proper treatment of the kinetics entails a lengthy calculation and tabulation of activation energies and estimation of pre-exponential factors, then construction of a surface reaction kinetic model coupled with mass transport effects and corrosion product formation. This is beyond our immediate scope, but consideration of the impetus conveyed to corrosion by these various thermodynamic driving factors is at the heart of the arguments constructed herein.

There are two cathodic reactions that commonly dominate aqueous electrochemical corrosion: the oxygen reduction reaction (ORR) and the hydrogen evolution reaction (HER).³⁶ Mixed Potential Theory provides a useful construct for estimating and interpreting electrochemical polarization curves for corrosion. It treats the metal dissolution kinetics independently from the accompanying reduction reaction kinetics.^{28,30} This fundamental understanding on the intersection point composed of the corrosion potential (E_{corr}) and corrosion current density (i_{corr}) as a result of two simultaneous operating reactions is schematically captured in Fig. 1 (left).

The Tafel approximation to the Butler-Volmer equation applied at potentials far away from the reversible potential relates the anodic current density i_a^0 to the applied potential E as follows:³⁶

$$i_a(E) = i_a^0 \cdot \exp \left[\frac{\beta n e (E - E_{\text{rev}})}{k_b T} \right] \quad [2]$$

where E_{rev} is the reversible electrode potential; i_a^0 is the exchange current density for the anodic reaction; e is the elementary charge constant; β is the symmetry coefficient; n is the number of charges transferred in the reaction; k_b is the Boltzmann constant; T is the temperature.

To develop the theoretical connection between the corrosion potential and the work function, we take the standard reversible potentials, E_{rev}^0 , as expressed in the reduction reaction, E_{red}^0 , in place of E_{rev} , which is equivalent to considering the reacting species to be in their standard state, by convention. The anodic kinetics captured in Eq. 2 demonstrate the contributions from the intrinsic metal reactivity, i_a^0 , as well as the electrochemical driving force, $(E - E_{\text{red}}^0)$, enclosed within the exponential term. To a first approximation, we treat these two terms as separable. Furthermore, we can neglect detailed treatment of the cathodic curve at this time, although that will also vary from metal to metal. With these assumptions in mind, we can consider that, to first order, the response of the corrosion potential E_{corr} to changes in ϕ_e , will primarily manifest through changes in the position of the anodic curve, such that a new intersection between anodic curve and cathodic curve is established, i.e. at the point (E_{corr} , i_{corr}). This relationship is depicted schematically in Fig. 1 (right).

Consistent with this line of argument, Li and Li reported an observation that the variation of ϕ_e and E_{corr} measured on a series of deformed Cu surfaces are correlated.³² When the plastic strain increased from 0 to 40%, measured ϕ_e decreased from 4.8 eV to 4.4 eV, meanwhile, measured E_{corr} decreased from -400 mV to -430 mV, and the corrosion rate continuously increased from 2.5 to 4.5 g mm⁻²s⁻¹, respectively. For the initially undeformed Cu surface, the measured E_{corr} would correspond to the blue circle in

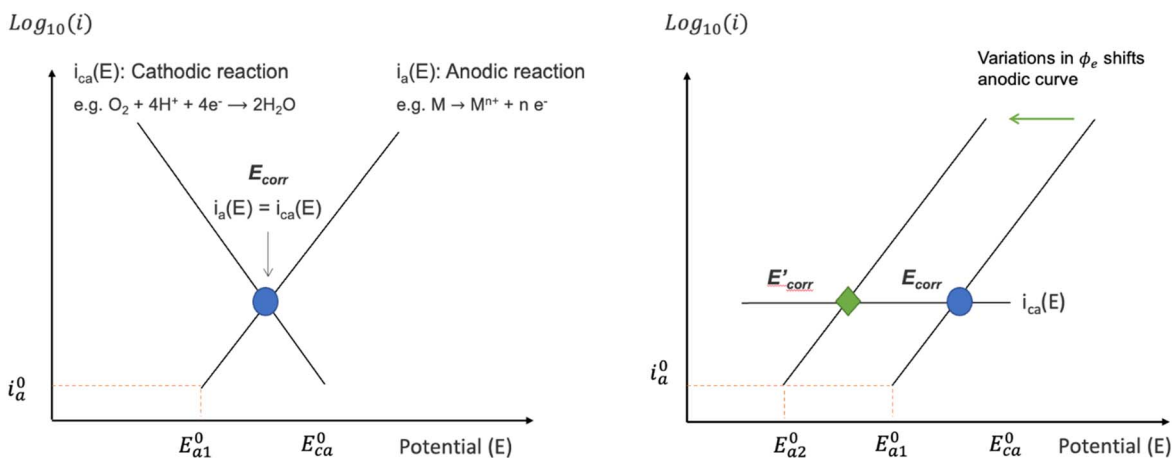


Figure 1. (left). Schematic representation of the Mixed Potential approach that determines the E_{corr} ; (right). Re-establishing E'_{corr} due to variations in ϕ_e . It is assumed that the cathodic kinetics are diffusion limited for ORR and i_a^0 is also constant. Under these assumptions E_{corr} is mainly controlled by E_{red}^0 .

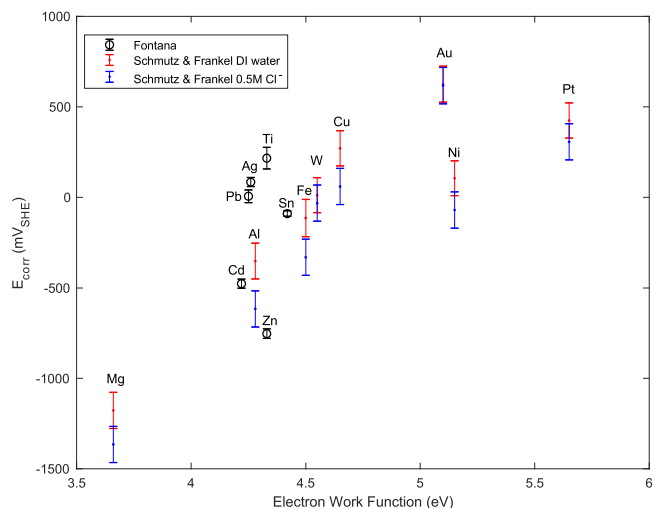


Figure 2. The E_{corr} vs the ϕ_e for 14 metals. For Schmutz and Frankel data collected in deionized water,²⁵ the best fit line is $E_{\text{corr}} = 804 \phi_e - 3797$ with $R^2 = 0.77$; in 0.5 M Cl^- , the best fit line is $E_{\text{corr}} = 867 \phi_e - 4246$ and $R^2 = 0.75$.

Fig. 1 (right). As a result of plastic deformation, the ϕ_e of the Cu surface decreases, as the change in work function effectively shifts the anodic curve, re-establishing the new E'_{corr} (green diamond). Despite the simplicity of the model, it accounts for the change in E_{corr} due to variations in the metal electronic state. Although it does not correctly account for the increase in i_{corr} , the difference in i_{corr} is on the same order of magnitude. We suggest that future improvement of the model may benefit from considering variations in ϕ_e that may also correlate with i_a^0 .

We extend this analysis to include more metals and re-evaluate to what extent a single-valued parameter ϕ_e may correlate with the kinetically controlled parameter E_{corr} , using experimental data collected from the literature.^{25,36} It is worth noting that the original data from Schmutz and Frankel were plotted using the Volta potential differences (referenced against a Ni probe) on the x -axis, and a linear correlation with $R^2 = 0.97$ was reported.²⁵ In Fig. 2, we extracted the same data points but plotted the E_{corr} against the corresponding polycrystalline ϕ_e instead.

The scatter of the data presented in Fig. 2 can be attributed to the kinetic factors. As Rohwerder and Turcu stated,²⁷ solution chemistry and double-layer effects contribute to the measured E_{corr} , and this is reflected through the differences between Schmutz and Frankel's two groups of data. Passive film properties will also have an effect.

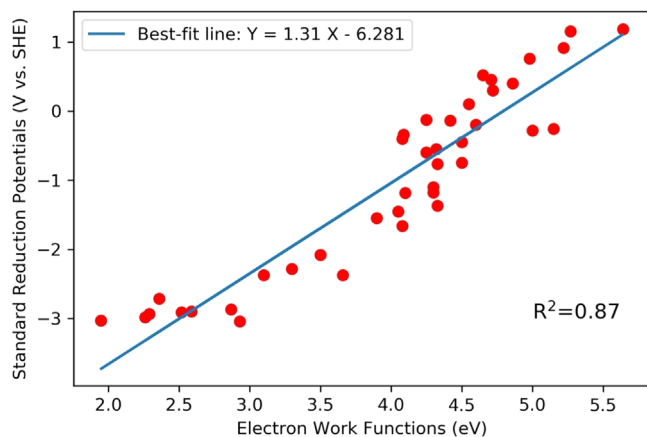


Figure 3. Correlation between work functions of 40 metals and their corresponding standard reduction potentials. The data are provided in Supporting Information (Tables SI and SII), and the annotated version of this figure is provided in Fig. S1 (available online at stacks.iop.org/JES/169/081506/mmedia). The experimental measurements are based on photoelectric and contact potential difference methods for the majority of metals contained herein.^{22,34} The three substantial outliers: Ag, Au, and Be are not included.

The presence of chloride anion in the solution consistently decreased the measured E_{corr} . Guillaumin et al. stated that the tightly correlated E_{corr} vs Volta potential difference is owing to the SKPFM capturing the effect of the surface charge, implying that the electric double layer may still be retained when the electrode was emersed out of solution.³⁸ Despite the scatter, the correlation of ϕ_e with the kinetically controlled E_{corr} can still be observed. Herein, we observe that the x -axis intercepts for deionized water and 0.5 M [Cl⁻] are approximately 4.72 and 4.90 V_{SHE}, respectively. We propose that the presence of the surface charge contribution to the Volta potential when the electrode is just emersed from solution may be considered a perturbation around the dominant effect of ϕ_e . Effectively then, the SKPFM provides a measure of the modified ϕ_e in the presence of a minimally retained layer of solvent. The concept of the modified ϕ_e has also been proposed by Gomer and Tryson, who reported a value of 4.73 V_{SHE}.³⁹ The extent to which this modification causes the measurement to deviate away from the ϕ_e is intrinsic to the interface structure between metal and solvent, because the water molecule dipole orientations,^{8,21,40} as well as other adsorbed anions,^{27,39} will play a role on the measurement of solvent modified ϕ_e .

A statistical and theoretical analysis of Gerischer's postulate.—

Gerischer's postulate, Eq. 1, proposed that E_{red}^0 and ϕ_e should exhibit a linear correlation (technically, the postulate refers to the Fermi level not work function, but the work function is the Fermi level relative to the vacuum level). Thus, it follows (via Mixed Potential Theory) that changes in ϕ_e would likewise have a carry-through effect on E_{corr} , since shifting ϕ_e will raise or lower the anodic curves in Fig. 1 (right). To directly evaluate Gerischer's postulate, we have compiled a list of ϕ_e and E_{red}^0 for 40 metals. The result is shown in Fig. 3.

The experimental measurements are based on photoelectric and contact potential difference methods for the majority of metals, and the thermionic method for a select few others. The detailed experimental methods and description are contained in the publication of Michaelson.^{22,34} The best fit line to describe the correlation between E_{red}^0 and ϕ_e is $E_{\text{red}}^0 = 1.31 \phi_e - 6.281$ with $R^2 = 0.87$. This equation intercepts the x -axis at approximately 4.79 eV, with the additional implication that this empirical equation predicts the standard hydrogen electrode (SHE), where $E_{\text{SHE}}^0 = 0$ V, to have an equivalent ϕ_e of 4.79 eV (i.e., this is the potential of the SHE on the vacuum electron scale). Note that, depending on the source of data,^{34,35,41,42}

both ϕ_e and E_{red}^0 will have some uncertainty and, therefore, intrinsic variation (scatter). Upon plotting different values for ϕ_e and E_{red}^0 , we report that the x -axis intercept has deviation on the order of ± 0.05 eV. In addition to the intrinsic variation, three substantial data outliers (e.g. Ag, Au, and Be) also contribute to the scattering. The reasons that give rise to these outliers, as explored by Trasatti, may be related to their unique metal/solvent interface structure.^{21,43} We will focus on the general trendline and the x -axis intercept that gives rise to the equivalent SHE ϕ_e , instead of discussing what makes each individual outlier unique, because we first seek to provide a basis for understanding the physics underlying this general correlation.

The SHE scale is the conventional reference point within the electrochemistry community. In the 1970s, efforts were dedicated to relating the SHE scale to an absolute scale referenced to the energy of the free electron in vacuum (i.e. an effective “work function” for the SHE). In a 1980s report for the IUPAC, Trasatti proposed the value of 4.44 ± 0.02 V.²⁹ This value is the result of an electrochemical cell set up that utilized the Hg electrode owing to its ideal polarizable surface. In the following years, different values have been arrived at, depending on the approach. For example, working with updated thermodynamic data, Fawcett measured $E_{\text{SHE(abs)}}^0 = 4.42$ V in H₂O solvent.⁴⁴ Kelly et al. reported $E_{\text{SHE(abs)}}^0 = 4.28$ V in H₂O solvent.⁴⁵ Donald et al. used mass spectrometry data for water droplets and estimated $E_{\text{SHE(abs)}}^0 = 4.2 \pm 0.4$ V.^{46,47} Gomer and Tryson employed the vibrating condenser method and reported $E_{\text{SHE(abs)}}^0 = 4.73 \pm 0.05$ V.³⁹ Pecina et al. also advocated $E_{\text{SHE(abs)}}^0 = 4.7$ V.⁴⁸ More recently, the advancement of aqueous solvation theory and computational modeling has helped to quantitatively capture the critical values in a simulation environment. Taylor et al.⁸ leveraged a Born-Haber thermodynamic cycle and the Sackur-Tetrode equation and calculated $E_{\text{SHE(abs)}}^0 = 4.51$ V at 0 K, $E_{\text{SHE(abs)}}^0 = 4.67$ V at 300 K, and $E_{\text{SHE(abs)}}^0 = 5.63$ V at 600 K, respectively using DFT at the revised Perdew–Burke–Ernzerhof (RPBE)⁴⁹ level of theory. Tripkovic et al. computed ab initio absolute standard hydrogen electrode potentials (i.e., $E_{\text{SHE(abs)}}^0$) for 8 transition metal surfaces. Their study investigated the effect of exchange correlation functional, namely Perdew–Burke–Ernzerhof (PBE) vs RPBE, tested four physical models of H₂O, and concluded that the static H₂O dipole effect and the extent of charge transfer between H₂O and metal surface both contributes to the calculated $E_{\text{SHE(abs)}}^0$. $E_{\text{SHE(abs)}}^0 = 4.68$ V was reproduced for the H₂O model without net dipole and charge transfer, whereas including the flexibility of the H₂O network in addition to no net dipole and charge transfer produced $E_{\text{SHE(abs)}}^0 = 4.30$ V.⁵⁰

Trasatti provided three ways of measuring $E_{\text{SHE(abs)}}^0$, but only one was amenable to practical measurement using the Hg electrode.^{29,51} On the other hand, estimating $E_{\text{SHE(abs)}}^0$ based on the Born-Haber cycle requires the computation or estimation of the H⁺ cation solvation energy. Depending on the techniques adopted to measure H⁺ hydration energy, this value can also differ by as much as 0.5 eV.⁵² Hence there remains some intrinsic circularity between knowing the $E_{\text{SHE(abs)}}^0$ and the single ion solvation energy. With this in mind, the fact that the best fit line in Fig. 3 intercepts the x -axis at $E_{\text{SHE(abs)}}^0 = 4.79$ V suggests that there is a physically meaningful connection underlying the relationship between E_{red}^0 and ϕ_e . Beyond this correlation, however, we aim in this work to provide a theoretical basis for the correlation by examining the underlying physical processes that occur during corrosion.

To this end, a Born-Haber cycle can be utilized to help break down a complex, aggregated, and multi-step but experimentally measurable property into elementary, tractable, and thermodynamically well-defined reaction sequences. The process of constructing a Born-Haber cycle can be especially useful in bridging the different

perspectives between experimentalists with a top-down view and theoreticians with a bottom-up modeling approach. Furthermore, it can be helpful in identifying the most energetically intensive components of a mechanism, which may give insight as to the rate-limiting step. Trasatti constructed a Born-Haber cycle to independently verify the experimentally measured $E_{\text{SHE(abs)}}^0$.²⁹ To estimate $E_{\text{SHE(abs)}}^0$, Trasatti's Born-Haber cycle involved the free energies of atomization of H_2 gas, G_{atm} , first ionization energy of atomic H gas, IE_{1st} , and ionic hydration free energy, G_{hyd} . The three steps involved can be summarized in Fig. 4 (left). Similarly, we can also adopt a Born-Haber cycle for each metal element that was considered earlier in Fig. 3. Such a Born-Haber cycle is shown in Fig. 4 (right). The cycle involves the removal of the metal atom from the lattice, the ionization of the metal to charge state n , and then the hydration of the metal ion to form the solvated cation.

When cohesive energies of metals (E_{coh}),^{53,54} ionization energies (IE),⁵⁵ and cation hydration free energies (G_{hyd})^{56,57} are available, we may also estimate the absolute electrode potential for metal M, given as

$$E_{\text{M}^{n+}/\text{M(abs)}}^0 = \frac{E_{\text{coh}} + \sum_{i=1}^n IE + G_{\text{hyd}}}{n \cdot e} \quad [3]$$

We compiled cohesive energies (E_{coh}),⁵⁵ ionization energies (IE),⁵⁸ and ionic hydration free energies (G_{hyd})^{56,57} for the metal elements presented in Fig. 3 (see Supporting Information Table SIII to Table SV for the compiled data). We normalized the sum of the three energies by the number of electrons involved for the electrochemical reduction reaction. The resulting correlation between the standard reduction potentials and this "absolute" potential determined from the theoretical summation, $E_{\text{M}^{n+}/\text{M(abs)}}^0$, is presented in Fig. 5.

The best fit line for Fig. 5 intercepts the x -axis at around 4.9 V. This value falls in the upper range of previously discussed $E_{\text{SHE(abs)}}^0$. Effectively, we may interpret the physical meaning of Fig. 5 as a theoretically informed and statistically averaged approach to independent calibration of the absolute potential of the hydrogen half-cell reaction. This approach yields $E_{\text{SHE(abs)}}^0$ that is within 0.2 V of the best-fit line from Fig. 3. Analysis of the source of E_{coh} , IE , and G_{hyd} and their uncertainties, suggests that the accuracy of IE is at least on the order of 0.01 electron volt (eV). On the other hand, the average uncertainty of G_{hyd} measurements for multivalent cations is ± 0.1 eV. E_{coh} data are given without uncertainty. We point out that Fig. 5 is constructed from a collection of 28 metal elements with well-documented E_{coh} , IE , and G_{hyd} . Later in this paper, we will utilize the relation in Fig. 5 to estimate G_{hyd} for the remaining 15 metal cations not included in Fig. 5.

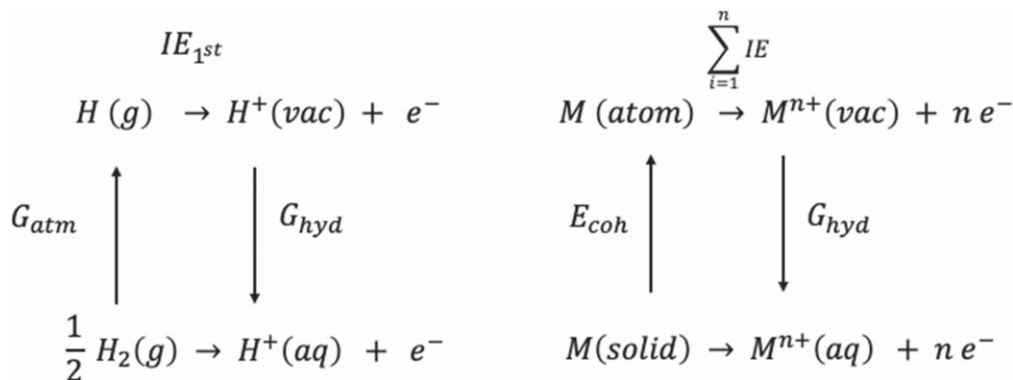


Figure 4. (left) Schematic Born-Haber cycle utilized by Trasatti to independently estimate and confirm the standard hydrogen electrode on an absolute scale;²⁹ (right) Schematic Born-Haber cycle for metal elements listed in Fig. 3.

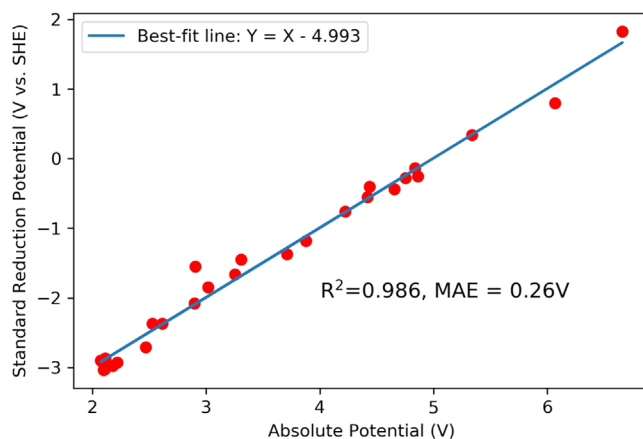


Figure 5. A correlation plot between E_{red}^0 and calculated absolute electrode potential (V) via Eq. 3. Equation 3 permits the calculation of absolute value of the standard hydrogen electrode because following the Born-Haber cycle (Fig. 4 right), the reference point is chosen as electrons resting at a point in vacuum. The annotated version of this figure can be found in Fig S2.

The role of the electronic and ionic work function in direct computation of standard reduction potentials.—The electronic work function, ϕ_e does not directly appear in the thermodynamic calculation of E_{red}^0 from the Trasatti-inspired Born-Haber cycle given in Fig. 6 (upper yellow route) or Eq. 3. However, the correlations presented in Figs. 2 and 3 suggest that there should be some kind of thermodynamic relationship that could be revealed with an alternative Born-Haber cycle for anodic dissolution. Such an alternative Born-Haber cycle can indeed be conceived, as illustrated in Fig. 6 (lower blue route).

In the first step, an electron (or multiple electrons for the situation in which a multivalent cation is formed) is (are) extracted from the Fermi level of the metal to a point in vacuum, leaving behind a conductive medium with an aggregate surface charge density δ^+ equivalent to the number of electrons removed (δ^+ indicates that the positive charge will be uniformly distributed across the metal surface). In the following step, a metal cation is then removed from the surface into the vacuum region, thus neutralizing the surface charge density on the metal. In the last step, the extracted cation is fully hydrated in solvent (e.g., H_2O), forming the solvation sheath. The sequence of energies required at each step are equivalent to $n \cdot \phi_e$ for step one, and the solvation free energy (G_{hyd}), for step three. Both values are well-documented in the literature.^{34,56,57} The energetic term describing the removal of an ion from the surface during the second step has not been significantly explored within the electrochemistry literature, which invites some original speculation here and the opportunity to make independent estimates for this

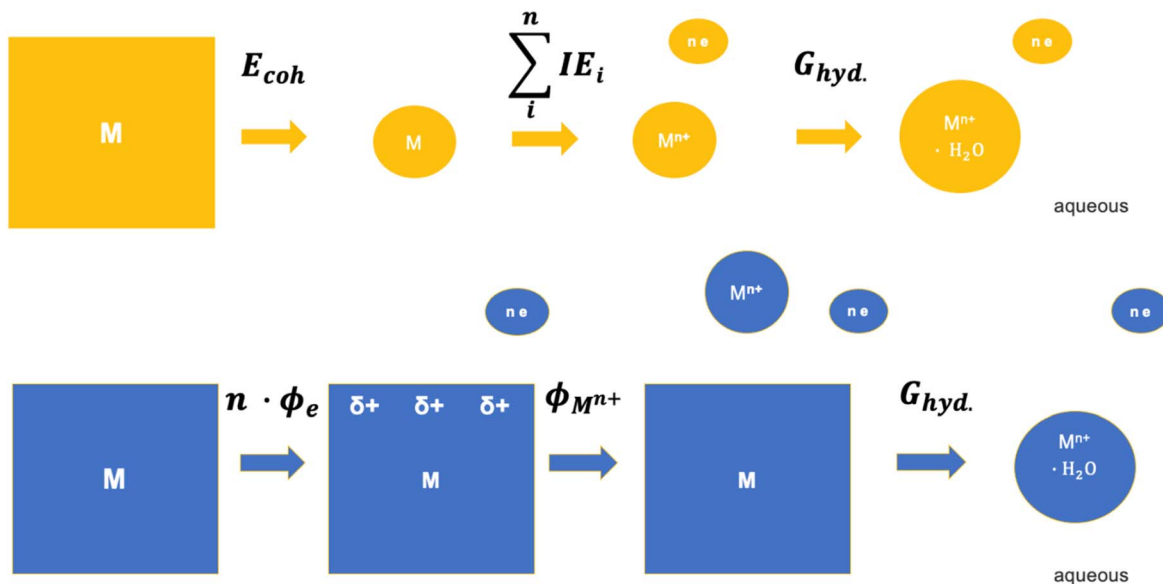


Figure 6. Two Born-Haber cycles to describe the underlying metal dissolution processes. The cubes represent the bulk surface of a metal and circles represent atoms, hydrated ions, and electrons. The conventional route (depicted in yellow) involves the breakdown of bulk metals into its constituent atoms, ionizing and then hydrating the atoms. The total energy of this process is $E_{\text{coh}} + \sum_{i=1}^n IE_i + G_{\text{hyd}}$. We propose an alternative route (depicted in blue) that purposefully integrates ϕ_e into the process. Following the extraction of electrons, the extraction of metal cations then neutralizes the bulk surface. The last step is the same as hydrating the metal cations in solution. The total energy of this process is $n \cdot \phi_e + \phi_{M^{n+}} + G_{\text{hyd}}$. Note that in both route, electrons are extracted to a point in vacuum where interactions with the metal is minimal.

quantity. We propose that the most descriptive term to capture the physical process in step two is ionic desorption,^{59,60} and the energy cost to quantify this action is best termed the ionic work function, $\phi_{M^{n+}}$.^{44,61} Therefore, we define the $\phi_{M^{n+}}$ as the minimum energy required to remove a surface cation into the vacuum just above the metal surface, following the removal of the corresponding number of electrons, for the surface to remain charge neutral.

In comparison to ϕ_e , $\phi_{M^{n+}}$ is the lesser explored concept when investigating metal dissolution reactions and, at least in the context of developing a first-principles mechanistic, as well as descriptor-based approach to corrosion, requires some elaboration. $\phi_{M^{n+}}$ in an aqueous environment can be challenging to directly measure. To a first approximation, we may estimate the values of $\phi_{M^{n+}}$ by equating the sum of energy terms from the two Born-Haber cycles. To be clear, the two cycles have the same beginning and endpoints, despite taking different pathways, and therefore their sum should be entirely equivalent, and can be expressed as

$$E_{\text{coh}} + \sum_{i=1}^n IE + G_{\text{hyd}} = n\phi_e + \phi_{M^{n+}} + G_{\text{hyd}} \quad [4]$$

Re-arranging the terms to solve for $\phi_{M^{n+}}$, we arrive at

$$\phi_{M^{n+}} = E_{\text{coh}} + \sum_{i=1}^n IE - n\phi_e \quad [5]$$

All three terms on the right-hand side of Eq. 5 are well-documented from independently conducted experiments, which allows estimation of $\phi_{M^{n+}}$ for many of the metallic elements (the use of DFT calculations for hypothetical alloys will create many more possibilities in the future). We also note that the hydration free energy G_{hyd} does not appear in this expression for the $\phi_{M^{n+}}$ because the third stage in the top sequence in Fig. 6 is notionally the same state as the third stage in the bottom sequence.

To independently test the accuracy of our estimated $\phi_{M^{n+}}$, we resort to a comprehensive and critically reviewed survey by Kawano on the topic of effective work functions for ionic and electronic thermal emission from polycrystalline surfaces.⁵⁹

Kawano stated that ϕ_e is the main factor governing not only thermal emission of electrons, but also positive and negative ion emission. He reported that the Schottky relation equates work function to the ion desorption energy. The original equation as first given by Schottky is,⁶⁰

$$\phi + E^+ = E^0 + IE \quad [6]$$

where ϕ is the electronic work function for clean monocrystalline surface, E^+ is the cation desorption energy, E^0 is the neutral ion desorption energy, and IE is the first ionization energy for the desorbed ion of interest. It is useful to rearrange this Schottky equation in the following form,

$$E^+ = E^0 + IE - \phi \quad [7]$$

Comparing Eqs. 5 and 7, the similarity is evident, even though the motivations are quite different. For Kawano, the purpose was to advocate for the use of the effective work function whenever the surface of interest is polycrystalline or contains a foreign adsorbate. Otherwise, the Schottky relation would not hold, and a difference of ΔE^* naturally arises. ΔE^* is given as,

$$\Delta E^* \equiv (E^0 + IE) - (E^+ + \phi) \quad [8]$$

where ΔE^* is defined as the energy difference between the first term $E^0 + IE$ and second term $E^+ + \phi$.

Kawano discussed the notable examples of W and Ta that, when directly using electronic work function for pristine and monocrystalline surfaces in place of what should have been polycrystalline samples, can lead to discrepancies in the Schottky relation, as reflected in $\Delta E^* \neq 0$ eV.⁵⁹ In the ΔE^* estimations, all four terms were sourced from independent studies. ϕ was determined by the slope of the electron thermal emission formula, and IE was obtained from handbooks of spectral series. Both E^0 and E^+ were determined from data on adsorption lifetimes. From Kawano's compiled sources, we can obtain independent experimental evaluation of E^+ for four monovalent refractory metal cations: W^+ , Ta^+ , Re^+ , and Mo^+ , as compiled in Table I.

Note the discrepancies between the values we have reported and those in the literature are on the order of a few tenths of an eV for W, Ta, and Re, similar to the magnitudes of variation in the reported values for the absolute hydrogen electrode potential. Experimental investigation into the positive ionic work function for Mo was discordant at first in the 1930's.^{61,62} Our estimation yields $\phi_{\text{Mo}^+} = 9.66$ eV.

However, we realize that for the thermal positive ion emission experiment on refractory elements, only the monovalent cation is reported. The stringent experimental conditions of high temperature (~ 2000 K) and ultra-high vacuum ($\sim 10^{-9}$ torr) impose a limitation that prevents us from comparing to the ionic work function of multi-valent cations. In order to test the validity of the extension of Eq. 5 to account for multi-valent cations, we take advantage of the utility presented by the lower Born-Haber cycle in Fig. 6, which gives an alternative estimation of $\phi_{\text{M}^{n+}}$ based on independently assessed values of half-cell reduction free energy G_{red}^0 ,⁴² hydration free energy G_{hyd} ,⁵⁷ and ϕ_e of polycrystalline metals,³⁴ given as

$$\phi_{\text{M}^{n+}} = G_{\text{red}}^0 - G_{\text{hyd}} - n \phi_e \quad [9]$$

The estimation of $\phi_{\text{M}^{n+}}$ from Eq. 9 should in theory arrive at the same values estimated via Eq. 5. This is indeed the case as seen from Fig. 7.

The relationship between the ionic work function and cation hydration energy.—Close examination of the ionic work function values reveals that, for instance, $\phi_{\text{Cr}^{3+}} = 44.81$ eV, a value that is seemingly unfavorable to produce Cr^{3+} cations (in vacuum) in the first place. However, we argue that in an aqueous environment, the presence of the solvent during metal dissolution is not merely as a spectator and/or dielectric medium, but it plays a critical role in stabilizing multi-valent cations through coordination of the metal cations to the nearby water molecules to form a strong solvation sheath. In fact, Gileadi and Kirwa-Eisner stated that for the electrochemical reaction of metal deposition, “the increase in total energy of the system, as caused by displacement of the hydrated ion from its initial state in the outer Helmholtz plane towards the metal, is compensated by the decrease in energy resulting from interaction with the surface.”⁶⁵ To apply this thinking to the reverse process of metal dissolution, we conjecture that the energy input to produce a metal cation should be largely compensated to a similar magnitude (even within $k_b T$ at room temperature), when the same metal cation becomes fully solvated.

To explore the extent to which the large energies for the $\phi_{\text{M}^{n+}}$ may be offset by hydration, we compare $\phi_{\text{M}^{n+}}$ vs $-G_{\text{hyd}}$ for commonly observed metal cations in aqueous media. The results are shown in Fig. 8.

From Fig. 8, a best-fit line can be drawn $-G_{\text{hyd}} = 1.05\phi_{\text{M}^{n+}} - 0.326$, with $R^2 = 0.996$. The data points fall into 4 groups, which can be best separated by the valence number of metal cations. For metal cations with valence number 1, the data points reside at the lower end of the best-fit line. As metal cation valence number increases, data points gradually move towards the higher end of the line. This plot provides a quantitative support to our second conjecture that, during metal active dissolution, the high energy required by $\phi_{\text{M}^{n+}}$ is largely offset through the action of hydration. Even more strikingly, the hydration energy is a very good estimator of $\phi_{\text{M}^{n+}}$ for the metal even though the thermodynamic action of desorbing a metal cation

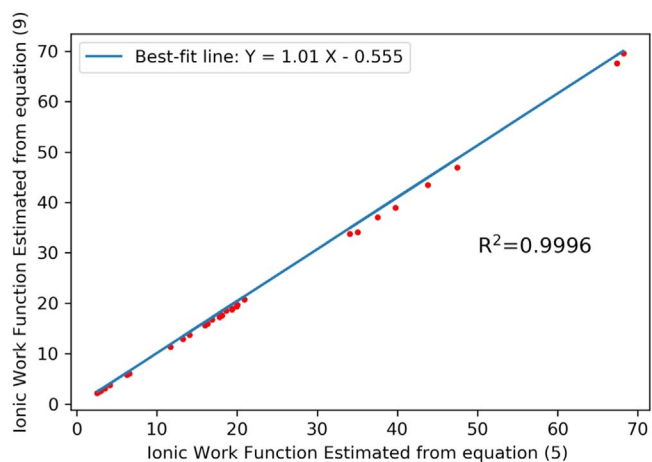


Figure 7. Two independent ways of estimating $\phi_{\text{M}^{n+}}$. The data points are comprised of 29 elements that have well documented E_{coh} , IE , ϕ_e , and G_{hyd} . For an annotated figure, see Fig S3 in Supporting Information. Note that to compute values of G_{red}^0 that are comparable to G_{hyd} and ϕ_e on the same scale, it is necessary to shift the reference from SHE to vacuum (i.e., using the SHE on the absolute scale). We adopted the absolute scale value of 4.9 V. The justification of using this value is born out of the x -axis intercept from Fig. 5.

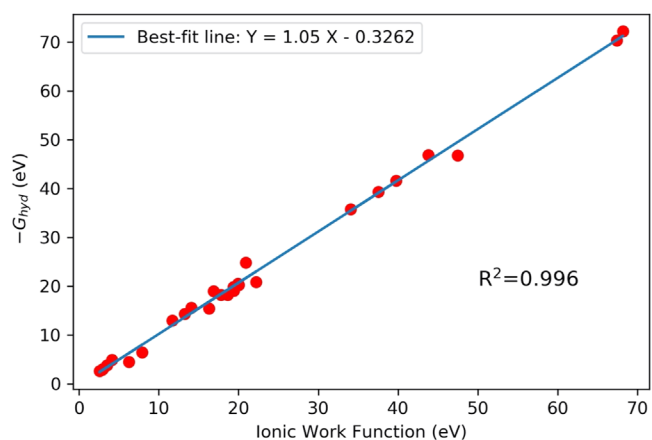


Figure 8. Correlation plot between $\phi_{\text{M}^{n+}}$ and $-G_{\text{hyd}}$ for 27 metals. These 27 data points are used as the training set (G_{hyd} for Cr^{3+} was excluded from the training set due to inaccurate reporting), where the best fit equation obtained from training will be used to make predictions on the remaining metals hydration free energies (see Table II). For an annotated figure, see Fig S4 in Supporting Information.

from the substrate $\phi_{\text{M}^{n+}}$ is endothermic in nature and the hydration energy is exothermic. Conversely, one could say that the expression in Eq. 5 is a good estimator of the hydration energy of the cation, despite only consisting of terms for the bulk metal (polycrystalline ϕ_e and E_{coh}) and the atomic properties of IE . The near equivalence between these two apparently different terms ($\phi_{\text{M}^{n+}}$ vs $-G_{\text{hyd}}$) relates to the conceptual similarity between them: *the energy for a metal cation to stabilize its electronic structure is of a similar order whether it is achieved by drawing a ligand field of water molecules, or interacting with its neighboring metal atoms in the metallic “sea of electrons” picture provided by jellium type models.*¹⁸

Since this correlation indicates that $\phi_{\text{M}^{n+}} \sim -G_{\text{hyd}}$, Eqs. 3 and 4 can be combined to yield the approximation that the absolute electrode potential is about equal to the electron work function:

$$E_{\text{M}^{n+}/\text{M}}^0 (\text{abs}) \sim \phi_e \quad [10]$$

This correlation is essentially borne out by the plot in Fig. 3, and yields the Gerischer conjecture once more, Eq. 1.

Table I. Comparison between ionic work function ϕ_{M^+} estimated via Eq. 5 and experiment measurements.^{59,62-64}

M^+	W^+	Ta^+	Re^+	Mo^+
ϕ_{M^+} (eV)	12.27	11.51	11.14	9.66
Exp. ϕ_{M^+} (eV)	12.1	11.2	10.7	8.6

A unique insight from the empirical relation between $\phi_{M^{n+}}$ vs $-G_{\text{hyd}}$ is that we may rely on the estimation of $\phi_{M^{n+}}$ to accurately predict the cation solvation free energy. Recall that Fig. 5 was constructed with a 28 of the total 43 metal elements that we have compiled. Part of the reason for the omission of some metal elements is owing to the unavailability of G_{hyd} data. We obtained G_{hyd} from the comprehensive compilation by Marcus,⁵⁷ and complemented it with cation hydration enthalpies (H_{hyd}), independently compiled by Smith.⁵⁶ Five metal elements (Ru, Re, W, Ir, and Ta) did not appear in either compilation. The reason for these five omissions is not commented on by either author. With the empirical equation obtained in Fig. 8, the remaining 10 metal elements (Pb, Pt, V, Tc, Mo, Rh, In, Lu, Nb, and Cr) are used for model validation. Herein, we have devised a validation approach that splits the dataset of 43 elements into three groups, a training dataset (Fig. 5), a testing dataset (Pb, Pt, V, Tc, Mo, Rh, In, Lu, Nb, and Cr), and 5 unknowns (Ru, Re, W, Ir, and Ta). The training set yields an empirical model shown in the best-fit line in Fig. 5. Next, we use the testing datasets to validate the two approaches of estimating G_{hyd} and attempt a theoretical estimation for the 5 unknowns with no available H_{hyd} or G_{hyd} . The first approach to predict G_{hyd} is based on reverse application of the empirical equation established from Fig. 5, and the second approach is based on the empirical equation established from Fig. 8 that relates $\phi_{M^{n+}}$ to the corresponding cation G_{hyd} . The two estimations for the 10 testing data and predictions for the 5 unknown data are provided in Table II.

For the Re^{3+} , Ir^{3+} , and Ta^{3+} predictions, we are only able to provide values to the nearest tenth of an eV since the precision is limited by the IE data. Upon close examination between Smith's and Marcus' compiled hydration data, we find inconsistency surrounding the Cr^{3+} hydration as the values reported by the two authors differ by 5.7 eV, which cannot be solely attributed to just the solvation entropy difference. To find which value is more reasonable, we estimated the Cr^{3+} solvation enthalpy and solvation free energy using the empirical equation obtained from the training dataset that excludes Cr^{3+} . The resulting predictions show closer agreement with Smith's value and indicate that Marcus' Cr^{3+} value is likely less accurate.

The correlation between the electron and ionic work functions.—Owing to the inherent challenge in independently measuring $\phi_{M^{n+}}$ in an aqueous environment, we explore some possible correlation between $\phi_{M^{n+}}$ and ϕ_e . The idea is to demonstrate that ϕ_e is a fundamental physical quantity that can be correlated with

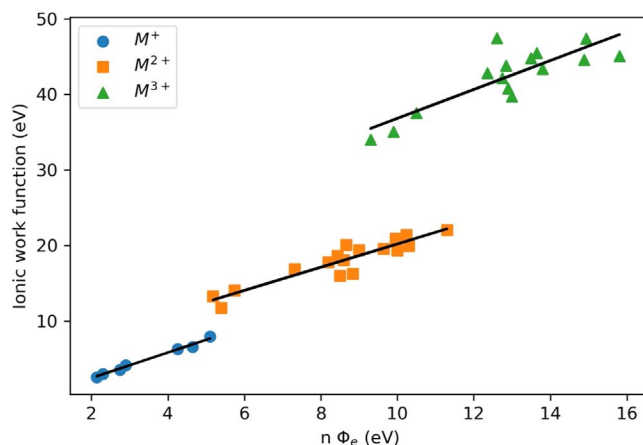


Figure 9. Electronic work functions and ionic work functions correlation. For mono-valent cations, the best-fit line yields an empirical correlation $\phi_{M^+} = 1.687 \phi_e - 0.938$, with $R^2 = 0.99$. For divalent cations, the best-fit line yields $\phi_{M^{2+}} = 1.538 \phi_e + 4.818$, with $R^2 = 0.86$. For trivalent cations, the best-fit line yields $\phi_{M^{3+}} = 1.915 \phi_e + 17.68$, with $R^2 = 0.71$. As cation valency number increases, the correlation becomes weaker, which suggests other parameters should be involved. For the annotated version of this figure, see Fig S5 in Supporting Information.

other electrochemical quantities, including, in this case, $\phi_{M^{n+}}$. A first attempt at correlating $\phi_{M^{n+}}$ and ϕ_e is shown in Fig. 9.

There is an evident clustering of the trends within Fig. 9 according to the cation valency. As cation valence increases, the predictability based solely from ϕ_e yields more uncertainties, as seen by the R^2 score (Fig. 9 caption). Based on these empirical correlations, ϕ_e can be used to directly predict ϕ_{M^+} of the matching metal, albeit with less accuracy for $\phi_{M^{2+}}$ and $\phi_{M^{3+}}$ than estimating it via Eq. 5. The insights obtained from Fig. 9 also suggest that ϕ_e is indeed a fundamental physical quantity that can be related to $\phi_{M^{n+}}$ among other terms. To explore the underlying physical relationship between ϕ_e and $\phi_{M^{n+}}$, we consider similar relations in the literature.

It has been recognized since the 1970s that the first IE and ϕ_e of the metal elements have an approximate correlation, as best captured by,^{66–68}

$$\frac{IE_1^{st}}{\phi_e} \approx 2 \quad [11]$$

Table II. Estimation of cation hydration free energies values via application of observed empirical equations obtained from Figs. 5 and 8, respectively.

Cations	G_{hyd} prediction via Fig. 5 (eV)	G_{hyd} prediction Fig. 8 (eV)	H_{hyd} (eV) from Smith ⁵⁶	G_{hyd} (eV) from Marcus ⁵⁷
Ru^{2+}	-19.96	-22.19	N/A	N/A
Pb^{2+}	-14.75	-16.45	-15.35	-14.77
Pt^{2+}	-21.02	-22.86	-21.77	N/A
Pd^{2+}	-19.84	-21.95	-20.61	-19.80
V^{2+}	-19.04	-18.65	-19.88	-18.92
Tc^{2+}	-18.60	-20.41	-19.26	N/A
Mo^{3+}	-42.82	-46.35	-44.46	N/A
Rh^{3+}	-45.10	-49.45	-46.59	N/A
Re^{3+}	-43.56	-47.2	N/A	N/A
In^{3+}	-41.24	-44.76	-42.62	N/A
W^{3+}	-43.86	-47.43	N/A	N/A
Ir^{3+}	-42.5	-47.0	N/A	N/A
Lu^{3+}	-36.58	-36.23	-36.59	-36.43
Nb^{3+}	-41.69	-41.54	-43.48	N/A
Ta^{3+}	-41.7	-43.9	N/A	N/A
Cr^{3+}	-45.56	-46.73	-47.26	-41.56

Wong et al. has proposed a simple image-charge force model that explains and reproduces this expected value of 2.⁶⁸ With our compiled data for both physical quantities across 43 metal elements, herein, we report a more generalized equation that extends beyond the first ionization process. Our generalized equation, observed by inspection, takes the following form:

$$\frac{\sum_{i=1}^n IE}{n \cdot \phi_e} \approx n + 1 \quad [12]$$

Equation 12 indicates that, for multivalent cations, the ratio of the sum of IE against $n \cdot \phi_e$ is expected to yield $(n + 1)$, and this expected value is 2 for a monovalent cation M^+ , which is the reduced form in Eq. 11. A table is provided in the Supporting Information (Table SVI) to support for our effort of generalization.

Recently, there has been a similar observation made within the battery research community of a correlation between E_{coh} and G_{red}^0 . Schmidt-Rohr, for instance, argued that the electrochemical energy released from a galvanic cell (e.g., Cu–Zn), is the manifestation of breaking the metal-metal bond energy stored in the form of the E_{coh} .⁶⁹ Founded on the concept of $\phi_{M^{n+}}$ and ϕ_e , we also explore how E_{coh} can also be correlated by utilizing Eq. 12. Based on our preceding discussions concerning the generalized form of Eq. 11, we propose that a unifying equation to capture the underlying relation amongst ϕ_e , $\phi_{M^{n+}}$, and E_{coh} can be expressed as

$$\phi_{M^{n+}} \approx n^2 \cdot \phi_e + E_{\text{coh}} \quad [13]$$

Equation 13 can be derived by substituting Eqs. 12 into 5 and replacing the sum of IE with the expression of $(n + 1) \cdot n \cdot \phi_e$. Equation 13 suggests that the energy required to initiate the metal dissolution reaction on an electrode is not only a function of the bulk metal-metal bond, which is captured by E_{coh} , but is also related to the electronic structure of the metal electrode, as described by ϕ_e . Exploring the extent to which our proposed relation is valid, we provide the plot shown in Fig. 10.

There are 4 groups that naturally arise from the resulting correlation, which correspond to the cation valency from +1 to +4. In addition, we used two colors (green for noble and orange for active) to indicate the individual electrochemical reactivity of each metal based on its standard reduction potential. Comparing the correlation obtained from Eq. 13 to that shown from Fig. 10, we find that incorporating the n^2 coefficient and the E_{coh} parameter has better unified the correlation between the ϕ_e and $\phi_{M^{n+}}$, especially for multivalent cations.

Discussion

A renewed perspective on corrosion through the work function.—Since the 1970s, ϕ_e has been theoretically used to infer the electrochemical activity of metals, even though ϕ_e does not appear explicitly in any electrochemical kinetics equations.²¹ More recently, however, with the advance and development of ab initio electrochemistry modeling, the utilizations of ϕ_e have been more explicit. For instance, Tripkovic et al. established the correlation between the potential of zero charge (PZC) and ϕ_e in an ab initio study.⁵⁰ For an ab initio corrosion approach, however, a similar correlation is wanting. The framework that we have presented in the preceding section re-examines the possibility of more concretely incorporating descriptors such as ϕ_e and $\phi_{M^{n+}}$ into models for dissolution thermodynamics and potentially for corrosion kinetics. In this section, we discuss how ϕ_e has been used in the current literature and how it can be leveraged to relate to corrosion kinetics through the mixed potential approach. We are particularly interested in how the descriptor may have a bearing on the application of DFT modeling to corrosion science.³

The relevance of ϕ_e in corrosion studies can be directly analyzed in a phenomenological way or interpreted within the Butler-Volmer

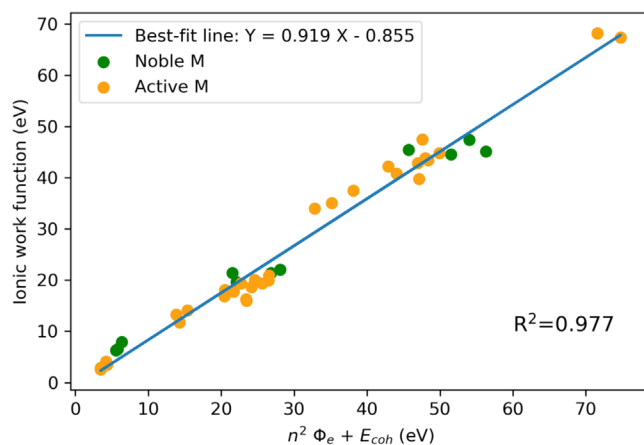


Figure 10. $\phi_{M^{n+}}$ vs $n^2 \cdot \phi_e + E_{\text{coh}}$ for 43 metals (previous outlier elements Au, Ag, and Be from Fig. 3 included herein). 4 groups naturally arise from this linear correlation that correspond to its cation valency from +1 to +4. These metals are also separated into two groups, noble vs active, differentiated based on the standard reduction potential on the SHE scale. For the annotated version of this figure, see Fig S6 in Supporting Information.

framework. On the experimental side, the series of works by Li and Li established a systematic understanding and correlation amongst the effects of metal surface morphology, measured ϕ_e via a scanning Kelvin probe, and observed copper surface corrosion kinetics.^{32,70–72} They tested the framework using a copper electrode and reported that as the copper surface is plastically deformed, the measured E_{corr} decreased, i_{corr} increased, and the measured ϕ_e decreased.³² On the simulation side using first principles method, Örnek et al. used DFT calculation of ϕ_e to characterize two intermetallic particles, Mg_2Si and Al_2Cu , that are present in high strength Al alloys.⁷³ Their DFT calculations indicate that surface termination can ultimately influence the magnitude and polarity of the Volta potential. As intermetallic surfaces are gradually covered by a monolayer of H_2O molecules, the calculated Volta potential suggests intermetallic particles undergo nobility inversions relative to the aluminum matrix. The DFT calculations agree with SKPFM measurements in predicting intermetallic particle nobility inversions as a function of relative humidity. Integrating both characterization and simulation approaches, Zhu et al. examined by transmission electron microscopy nm-scale T_B ($\text{Al}_{7.5}\text{Cu}_4\text{Li}$) intermetallic particles before and after corrosion testing and reported that T_B particle corrosion first initiated along the {001} plane, then propagated along the {110} and {111} family of planes.⁷⁴ Using DFT calculations of ϕ_e , they reported that the {001} plane is more electrochemically active owing to having a lower ϕ_e than the {110} and {111} surfaces, which explains the observed phenomenon of initial dissolution along the {001} plane prior to the others. Zhu et al. stated that since the {001} surface of T_B has the lowest value of ϕ_e amongst the three surfaces, it is expected to also have the lowest E_{corr} . Implicit to this interpretation is an underlying assumption that the E_{corr} for the intermetallic particles and matrix should be quantitatively related to the ϕ_e .

The term ionic work function originated from Fawcett's work, which characterizes the Gibbs free energy of extracting a hydrated ion from solvent into the gas phase, shedding the solvation sheath in the process.⁴⁴ According to Fawcett, the first reported experiment to measure the ionic work functions of hydrated ions were carried out by Kenrick,⁷⁵ hence the experimental apparatus was named the Kenrick cell. Leveraging the Kenrick cell, Fawcett was able to eliminate the Volta potential drop across interface and obtain the real potential of a proton, and with it the absolute electrode potential of SHE. Using the ionic work function to describe the Gibbs free energy of moving metal cations away from their surface substrate, as depicted by the alternative Born-Haber route in Fig. 6, we broaden

the utility of this concept to account for metal dissolution, and with it a new perspective on corrosion. Within the current framework, we have only tested the predictive correlation between $\phi_{M^{n+}}$ and its corresponding G_{hyd} . No oxo-metal or hydroxo-metal ion hydration free energy is considered. For future model development, a comprehensive and robust tabulation of oxo- and hydroxo-metal ion hydration free energy or enthalpy is needed. A recent grand canonical model development by Todorova and Neugebauer has made this endeavor possible via an ab initio method.¹⁴

Beyond the utilization by Fawcett, to the best of our knowledge, the ionic work function has not been explored within the context of corrosion science, but there are applications where it could be utilized.⁷⁶ Nevertheless, we believe that this should be the proper concept to treat the identity of charge carriers crossing the electric double layer in an anodic half reaction, as has been advocated by Gileadi and Kirova-Eisner.⁶⁵

Concluding Remarks

In this communication, we have reviewed and discussed several DFT studies that recognized the potential of ϕ_e to enhance our understanding of corrosion on an atomistic scale. We have shown that ϕ_e and $\phi_{M^{n+}}$ are useful indicators that can be used to construct the reaction energy landscape, particular concerning the standard reduction potential, and from mixed potential theory, have an effect of E_{corr} . To push for the development of a new corrosion kinetic framework, we echo the opinion of Trasatti that work functions should play an integral part in the accurate representation of the metal deposition and dissolution reactions.²¹ As for the identity of the charge carrier crossing the double layer, we advocate the view of Gileadi and Kirova-Eisner on metal cations as the charge carrier in metal dissolution and deposition reactions.⁶⁵ We contend that $\phi_{M^{n+}}$ provides a unique concept that can be applied to assist in characterizing this special class of electrochemical reactions.

Five key findings from this new perspective are summarized in the following points.

1. A general correlation between E_{red}^0 and ϕ_e has been reported in this communication, and the implications of this correlation have been presented and discussed in the context of aqueous corrosion reaction. An overlooked parameter is the ionic work function, $\phi_{M^{n+}}$, which naturally arises from the analysis of the two Born-Haber cycles. This parameter characterizes the energy penalty of creating metal cations in the vacuum.
2. The values for $\phi_{M^{n+}}$ have only been measured and reported on a group of selective metals with high melting points (W, Ta, Re, and Mo) in vacuum. In an aqueous electrochemical reaction, however, the measurements are not readily accessible, but we have shown that from the theoretical analysis, $\phi_{M^{n+}}$ is highly correlated with the single cation solvation energy and may even serve as a reliable descriptor for the prediction of single cation hydration energy.
3. Within the framework proposed by Gileadi on the actual charge transfer reaction in the metal dissolution/deposition type reactions, $\phi_{M^{n+}}$ can be a useful parameter to assess the reaction thermodynamics. The utility of $\phi_{M^{n+}}$ may also be found in using DFT to efficiently estimate the metal dissolution activation energy, a critical quantity that relates the thermodynamics to kinetics in the transition state theory.
4. Despite the intrinsic challenges embedded in independent measurement of $\phi_{M^{n+}}$, we have demonstrated that this quantity is also correlated with ϕ_e , a quantity that can be independently measured via the photoelectron experiment or computed in DFT.
5. We have also demonstrated that ϕ_e , a thermodynamically well-defined and measured quantity, intrinsically influences the electrode potential, and this correlation carries through to influence the measured corrosion potential, E_{corr} , a kinetically controlled parameter that is central to the thermodynamics of

corrosion reactions. We understand that, in our first attempt at drawing the correlation between ϕ_e and E_{corr} , many kinetic factors need to be strictly controlled for the statistical relationship to bear out. Therefore, this general framework may not be readily suitable to analyse a particular corrosion system where a dominant effect could be kinetically controlled. However, the “carry-through” effect can be effectively leveraged as a descriptor for high throughput computational approach for corrosion resistant alloy design in an integrated computational materials engineering (ICME) framework.

Acknowledgments

This work is supported by Office of Naval Research under the program manager Dr. Airan Perez, under the contract #N00014-18-1-2577. Any opinions, findings, and conclusions or recommendations expressed in this material are those of the author(s) and do not necessarily reflect the views of the Office of Naval Research. Sirui Li would like to express gratitude towards Dr. Tianshu Li and Dr. Huibin Ke. for stimulating discussions and providing constructive feedbacks during the manuscript preparations. Sirui Li would also like to thank Kaylee Ye for helpful suggestions and editing the abstract. Finally, Sirui Li would like to acknowledge the late Professor Eliezer Gileadi, whose forethought regarding the reversible processes between metal corrosion and deposition laid out the foundational hypothesis for this work.

ORCID

Sirui Li  <https://orcid.org/0000-0002-0206-8151>

References

1. C. D. Taylor and B. M. Tossey, *Npj Mater. Degrad.*, **5**, 38 (2021).
2. C. Nyby et al., *Sci. Data*, **8**, 58 (2021).
3. Y. Wang et al., *Adv. Sci.*, **9**, 2200370 (2022).
4. H. Ma, X. Q. Chen, R. Li, S. Wang, J. Dong, and W. Ke, *Acta Mater.*, **130**, 137 (2017).
5. B. Malki, I. Guillotte, and B. Baroux, *J. Electrochem. Soc.*, **165**, C703 (2018).
6. B. Malki, I. Guillotte, and B. Baroux, *J. Electrochem. Soc.*, **166**, C564 (2019).
7. C. D. Taylor and M. Neurock, *Curr. Opin. Solid State Mater. Sci.*, **9**, 49 (2005).
8. C. Taylor, R. G. Kelly, and M. Neurock, *J. Electrochem. Soc.*, **153**, E207 (2006).
9. J. A. Yuwono, N. Biribilis, C. D. Taylor, K. S. Williams, A. J. Samin, and N. V. Medhekar, *Corros. Sci.*, **147**, 53 (2019).
10. H. Ke, T. Li, P. Lu, G. S. Frankel, and C. D. Taylor, *J. Electrochem. Soc.*, **167**, 111501 (2020).
11. H. Ke and C. D. Taylor, *J. Electrochem. Soc.*, **167**, 111502 (2020).
12. C. D. Taylor, *Chem. Phys. Lett.*, **469**, 99 (2009).
13. H. Ke and C. D. Taylor, *J. Electrochem. Soc.*, **167**, 131508 (2020).
14. M. Todorova and J. Neugebauer, *Phys. Rev. Appl.*, **1**, 014001 (2014).
15. T. Duong, Y. Wang, X. Yan, A. Couet, and S. Chaudhuri, (2021), arXiv:2104.10590v1.
16. J. O. Bockris and A. K. N. Reddy, *Modern Electrochemistry* (Plenum Publishing Corporation, New York, NY) 1 (1970).
17. J. O. Bockris, B. E. Conway, and E. Yeager, *Comprehensive Treatise of Electrochemistry, Volume 1: The Double Layer*, (Plenum Press, New York, NY) (1980).
18. A. Kiejna and K. F. Wojciechowski, *Metal Surface Electron Physics, chapter 4: Electrons in Metals* (Elsevier, Amsterdam) (1996).
19. W. Schmickler and E. Santos, “A few basic concepts.” *Interfacial Electrochemistry*. (Springer, Berlin, Heidelberg) p. 29 (2010).
20. P. J. Gellings and H. J. M. Bouwmeester, *The CRC Handbook of SOLID STATE Electrochemistry* (CRC Press, Boca Raton, FL) (2019).
21. S. Trasatti, *J. Electroanal. Chem.*, **39**, 163 (1972).
22. H. B. Michaelson, *IBM J. Res. Dev.*, **22**, 72 (1978).
23. H. Kita and T. Kurisu, *J. Res. Inst. Catal. Hokkaido Univ.*, **21**, 200 (1974).
24. M. Stratmann, *Corros. Sci.*, **27**, 869 (1987).
25. P. Schmutz, *J. Electrochem. Soc.*, **145**, 2285 (1998).
26. Y. Martin, D. W. Abraham, and H. K. Wickramasinghe, *Appl. Phys. Lett.*, **52**, 1103 (1988).
27. M. Rohwerder and F. Turcu, *Electrochim. Acta*, **53**, 290 (2007).
28. F. Mansfeld, *Corrosion*, **62**, 843 (2006).
29. S. Trasatti, *Pure Appl. Chem.*, **58**, 955 (1986).
30. C. Wagner and W. Traud, *Z. Elektrochem.*, **44**, 391 (1938).
31. G. S. Frankel, “Wagner-Traud to Stern-Geary: Development of Corrosion Kinetics.” *ECS Meeting*, Philadelphia (2002).
32. W. Li and D. Y. Li, *Appl. Surf. Sci.*, **240**, 388 (2005).
33. H. Gerischer, *Surf. Sci.*, **18**, 97 (1969).
34. H. B. Michaelson, *J. Appl. Phys.*, **48**, 4729 (1977).

35. D. Lide, *CRC Handbook of Chemistry and Physics* (Taylor & Francis, Boca Raton, FL) (2008).
36. E. Mccafferty, *Introduction to Corrosion Science* (Springer, New York, NY) (2004).
37. S. Evans and E. L. Koehler, *J. Electrochem. Soc.*, **108**, 509 (1961).
38. V. Guillaumin, P. Schmutz, and G. S. Frankel, *J. Electrochem. Soc.*, **148**, B163 (2001).
39. R. Gomer and G. Tryson, *J. Chem. Phys.*, **66**, 4413 (1977).
40. C. D. Taylor, S. A. Wasileski, J. S. Filhol, and M. Neurock, *Phys. Rev. B - Condens. Matter Mater. Phys.*, **73**, 1 (2006).
41. S. Bratsch, *J. Phys. Chem. Ref. Data*, 1 (1989).
42. M. H. Weik, "Electrochemical series." *Computer Science and Communications Dictionary*. (Springer, Boston, MA) p.489 (2000).
43. S. Trasatti, *Electrochim. Acta*, **36**, 1659 (1991).
44. W. R. Fawcett, *Langmuir*, **24**, 9868 (2008).
45. C. P. Kelly, C. J. Cramer, and D. G. Truhlar, *J. Phys. Chem. B*, **110**, 16066 (2006).
46. W. A. Donald and E. R. Williams, *Pure Appl. Chem.*, **83**, 2129 (2011).
47. W. A. Donald, R. D. Leib, J. T. O'Brien, M. F. Bush, and E. R. Williams, *J. Am. Chem. Soc.*, **130**, 3371 (2008).
48. O. Pecina, W. Schmickler, and E. Spohr, *J. Electroanal. Chem.*, **394**, 29 (1995).
49. B. Hammer, L. B. Hansen, and J. K. Nørskov, *Phys. Rev. B*, **59**, 7413 (1999).
50. V. Tripkovic, M. E. Björketun, E. Skúlason, and J. Rossmeisl, *Phys. Rev. B*, **84**, 115452 (2011).
51. S. Trasatti, *Electrochim. Acta*, **35**, 269 (1990).
52. M. D. Tissandier, K. A. Cowen, W. Y. Feng, E. Gundlach, M. H. Cohen, A. D. Earhart, J. V. Coe, and T. R. Tuttle, *J. Phys. Chem. A*, **102**, 7787 (1998).
53. C. Kittel, *Introduction to Solid State Physics* (Wiley, New York, NY) (2004).
54. E. Kaxiras, *Atomic and Electronic Structure of Solids* (Cambridge University Press, Cambridge) (2003).
55. E. Mechtly, "Properties of Elements." *Elementary Materials Science* (ASM International, Materials Park, Ohio) p. 161 (2013).
56. D. W. Smith, *J. Chem. Educ.*, **54**, 540 (1977).
57. Y. Marcus, *J. Chem. Soc., Faraday Trans.*, **89**, 713 (1993).
58. NIST Atomic Spectra Database Ionization Energies Form <https://physics.nist.gov/PhysRefData/ASD/ionEnergy.html>.
59. H. Kawano, *Prog. Surf. Sci.*, **83**, 1 (2008).
60. W. Schottky, *Ann. Phys.*, 62 (1920).
61. L. Smith, *Phys. Rev.*, **35**, 381 (1930).
62. R. W. Wright, *Phys. Rev.*, **60**, 465 (1941).
63. M. D. Scheer and J. Fine, *J. Chem. Phys.*, **46**, 3998 (1967).
64. M. D. Scheer and J. Fine, *Proceedings of the 4th International Materials Symposium*, Berkeley 1968 (1968), pp. 39-1-15.
65. E. Gileadi and E. Kirova-Eisner, *Corros. Sci.*, **47**, 3068 (2005).
66. C. F. Gallo and W. L. Lama, *IEEE Trans. Ind. Appl. IA-10*, **496**, 496-500 (1974).
67. A. Rose, *Solid State Commun.*, **45**, 859 (1983).
68. K. Wong, S. Vongehr, and V. V. Kresin, *Phys. Rev. B - Condens. Matter Mater. Phys.*, **67**, 1 (2003).
69. K. Schmidt-Rohr, *J. Chem. Educ.*, **95**, 1801 (2018).
70. W. Li and D. Y. Li, *Acta Mater.*, **53**, 3871 (2005).
71. W. Li and D. Y. Li, *Acta Mater.*, **54**, 445 (2006).
72. W. Li and D. Y. Li, *J. Chem. Phys.*, **122**, 064708 (2005).
73. C. Örnek, C. Leygraf, and J. Pan, *Corros. Eng. Sci. Technol.*, **54**, 185 (2019).
74. Y. Zhu, J. D. Poplawsky, Sirui. Li, R. R. Unocic, L. G. Bland, C. D. Taylor, J. S. Locke, E. A. Marquis, and G. S. Frankel, *Acta Mater.*, **189**, 204 (2020).
75. F. B. Z. Kenrick, *Phys. Chem.*, **19**, 625 (1896).
76. Sirui. Li, *Multi-Physics Frameworks for Predicting Corrosion Thermodynamics, Kinetics, and Susceptibility from Density Functional Theory*, The Ohio State University (2021), https://etd.ohiolink.edu/apexprod/rws_etd/send_file/send?accession=osu1623203208454272&disposition=inline.